Statistics of the turbulent kinetic energy dissipation rate and its surrogates in a square cylinder wake flow

N. Lefeuvre, F. Thiesset, L. Djenidi, R. A. A Antonia

Statistics of the turbulent kinetic energy dissipation rate and its surrogates in a square cylinder wake flow

N. Lefeuvre,[1] F. Thiesset,[1] L. Djenidi,[1] and R.A. Antonia[1]

School of Engineering, University of Newcastle, Australia

(Dated: 5 April 2019)

A numerical simulation based on the lattice Boltzmann method is carried out in the wake of a square cylinder with the view to investigating possible surrogates for the instantaneous turbulent kinetic energy dissipation rate, ϵ, as well as its mean values, $\overline{\epsilon}$. Various surrogate approximations of ϵ, based on local isotropy (ϵ_{iso}), local axisymmetry along x ($\epsilon_{a,x}$) and y ($\epsilon_{a,y}$), local homogeneity (ϵ_{hom}), and homogeneity in the transverse plane, (ϵ_{4x}), are assessed.

All the approximations are in agreement with $\overline{\epsilon}$ when the distance downstream of the obstacle is larger than about 40 diameters. Closer to the obstacle, the agreement remains reasonable only for $\overline{\epsilon}_{a,x}$, $\overline{\epsilon}_{hom}$ and $\overline{\epsilon}_{4x}$.

The probability density functions (PDF) and joint PDFs of ϵ and its surrogates shows that ϵ_{4x} correlates best with ϵ while ϵ_{iso} shows the smallest correlation.

The results indicate that ϵ_{4x} is a very good surrogate for ϵ and can be used for correctly determining the behaviour of ϵ .

PACS numbers: 47.27.-i, 47.27.W-, 47.27.E-

Keywords: Numerical simulation, Wake, Dissipation rate

I. INTRODUCTION

The mean turbulent kinetic energy dissipation rate $\overline{\epsilon}$ is a fundamental quantity in turbulent flow studies. $\overline{\epsilon}$ is given by

$$\overline{\epsilon} = 2\nu\overline{s_{ij}s_{ij}}, \tag{1}$$

where $s_{ij} = 1/2\,(u_{i,j} + u_{j,i})$ is the fluctuating strain rate, ν is the kinematic viscosity, u_i is the fluctuation part of the velocity in the direction x $(i = 1)$, y $(i = 2)$, z $(i = 3)$ and $u_{i,j} \equiv \partial u_i/\partial x_j$ is the derivative of the velocity component u_i along the direction j. Since the groundbreaking work of Kolmogorov[19,20], it is widely recognized that $\overline{\epsilon}$ plays a crucial role in the theoretical study of small-scale turbulence[29], such as in spectral analysis and two-point spatial analysis. An accurate estimation of $\overline{\epsilon}$ is further essential for example in the context of closure models for the turbulent kinetic energy equation.

The estimation of $\overline{\epsilon}$ requires the knowledge of 12 terms. While all of these terms can be easily obtained from direct numerical simulation data, only a few of them can be measured from single-point time signals and using the Taylor hypothesis. Generally, it is the isotropic expression $\overline{\epsilon}_{iso}$ which is measured to approximate $\overline{\epsilon}$. It is a considerable simplification to Eq. (1) and is given by

$$\overline{\epsilon}_{iso} = 15\nu\overline{(u_{1,1})^2}. \tag{2}$$

However, while Eq. (2) may be appropriate in many circumstances where local isotropy is approximately satisfied (e.g. homogeneous and isotropic turbulence or HIT, centreline of wakes and jet, at a sufficiently large distance from the wall in pipe, channel and turbulent flows), this is not the case in general when the anisotropy of the flow is not negligible. For example, Browne et al.[6], who measured nine components of Eq. (1) and inferred the remaining three, showed that $\overline{\epsilon}_{iso}$ is not satisfied in the far-field of a circular cylinder wake (CC); $\overline{\epsilon}_{iso}$ was about 45% smaller than $\overline{\epsilon}$. Their results are consistent with those of Fabris[14] and Aronson and Lofdahl[5].

Another simplification can be made for estimating Eq. (1) if local homogeneity is satisfied. Under this condition and using the relation (22) given by Taylor[32], the locally homogeneous expression for the dissipation rate is

$$\overline{\epsilon}_{hom} = \nu\overline{\omega^2}. \tag{3}$$

where $\overline{\omega^2}$ is the enstrophy ($\equiv \overline{\omega_1^2} + \overline{\omega_2^2} + \overline{\omega_3^2}$). In deriving Eq. (3) the hypothesis $\overline{\nabla^2 p} = 0$ is used since Eq. (1) can be written as follows:

$$\overline{\epsilon} = 2\nu \left(\frac{\overline{\omega^2}}{2} - \overline{\nabla^2 p} \right) \tag{4}$$

At this stage, it seems clear that the difference between $\overline{\epsilon}$ and $\overline{\epsilon}_{hom}$ is related to the influence of pressure fluctuations in the flow under consideration. In the near[25] and far[6] fields of the CC wake, the experimental data show that $\overline{\epsilon}_{hom}$ is an accurate surrogate for $\overline{\epsilon}$. From an experimental viewpoint, this is of great interest because only nine velocity gradients need to be measured to obtain $\overline{\omega^2}$ and thus $\overline{\epsilon}_{hom}$.

Local axisymmetry, which is next to isotropic in order of simplicity but which occurs more commonly in practice, can also be invoked for estimating the energy dissipation rate. George and Hussein[16] were first to write the expressions for $\overline{\epsilon}_{a,x}$. If local axisymmetry along the axis x_1 is assumed then[17],

$$\overline{\epsilon}_{a,x} = \nu \left[-\overline{(u_{1,1})^2} + 2\overline{(u_{1,2})^2} + 2\overline{(u_{2,1})^2} + 8\overline{(u_{2,2})^2} \right] \tag{5}$$

Local axisymmetry with respect to the direction y can also be assumed, which leads to[33],

$$\overline{\epsilon}_{a,y} = \nu \left[8\overline{(u_{1,1})^2} + 2\overline{(u_{1,2})^2} + 2\overline{(u_{2,1})^2} - \overline{(u_{2,2})^2} \right]. \tag{6}$$

Finally, a fourth surrogate for the turbulent kinetic energy dissipation rate has been proposed by Zhu and Antonia[3,36]. These authors used a vorticity probe comprising 4 X-probes to measure all the velocity derivatives simultaneously, except $\overline{(u_{2,2})^2}$ and $\overline{(u_{3,3})^2}$. The incompressibility condition $u_{1,1} + u_{2,2} + u_{3,3} = 0$ led to the following relation

$$\overline{(u_{2,2})^2} + \overline{(u_{3,3})^2} = \overline{(u_{1,1})^2} - 2\overline{(u_{2,2})\,(u_{3,3})}. \tag{7}$$

Assuming homogeneity in the transverse plane $(y - z)$,

$$\overline{u_{2,2}u_{3,3}} = \overline{u_{2,3}u_{3,2}}. \tag{8}$$

Using Eqs. (7) and (8) leads to the following expression

$$\overline{\epsilon}_{4x} = \nu \Bigg[4\overline{(u_{1,1})^2} + \overline{(u_{1,2})^2} + \overline{(u_{1,3})^2} + \overline{(u_{2,1})^2} + \overline{(u_{2,3})^2} + \overline{(u_{3,1})^2} + \overline{(u_{3,2})^2} + 2\overline{(u_{1,2}u_{2,1})} + 2\overline{(u_{1,3}u_{3,1})} - 2\overline{(u_{2,3}u_{3,2})} \Bigg]. \tag{9}$$

The above $\overline{\epsilon}$-surrogate should strictly be valid if local homogeneity holds. However, both experimental[31,36] and numerical[10] data reveal its range of validity may be more general. For example, in the intermediate field, Thiesset[33] showed that $\overline{\epsilon}_{iso}$, $\overline{\epsilon}_{a,y}$ and $\overline{\epsilon}_{hom}$ are good candidates for estimating $\overline{\epsilon}$. In the far field of a CC wake, Hao et al.[35] showed that, near the wake centerline, $\overline{\epsilon}_{iso}$ was only about 10% smaller than $\overline{\epsilon}$, as measured by Browne et al.[6]. This contrasts with the measurements of Browne et al.[6] who, as previously mentioned, found that $\overline{\epsilon}_{iso}$ is about 45% smaller that $\overline{\epsilon}$. These inconsistent results highlight the difficulty of measuring $\overline{\epsilon}$ reliably. Even though $\overline{\epsilon}_{iso}$ can be suited in many situations, this does not necessarily imply that local isotropy holds. Indeed, in grid turbulence, Antonia et al.[4] showed that the velocity derivatives ratios differ from isotropy. However they remarked that there are some compensation effects among the 12 components of $\overline{\epsilon}$ which altogether allow the use of $\overline{\epsilon}_{iso}$. Similar observations were in a wake of different obstacles[34].

Moreover, the intermittent character of the velocity derivatives may play a role in the instantaneous distributions of surrogates for ϵ. Indeed, in the original K41 framework[19,20], the universality of the inertial range was proposed by supposing the latter being uniquely determined by $\overline{\epsilon}$. However, Landau[22] was first to comment that the energy dissipation rate has to be considered as a fluctuating quantity, in the same manner as any other fluctuating quantity. Since the fluctuations of ϵ are likely to be affected by the non-homogeneous large scales, the concept of universality may break down even for small scales. This behaviour, usually designated as internal intermittency has led to an explosion in publications over the last fifty years. Attention has been paid mostly to the deviation of scaling exponents to the original K41 predictions. However, the effect of fluctuations in the energy dissipation rate due to the large scales has been given much less attention, even though it is the essence of Landau's original comment. Therefore, not only the mean values but also the instantaneous behaviour of the dissipation rate is a major importance for giving some insight into the intermittent nature of turbulence.

Whilst numerical simulation is the most unambiguous tool for assessing the dissipation rate, the universality of turbulence can be only confirmed or invalidate at very high Reynolds numbers. Such high values of Reynolds numbers remain beyond the actual computing capabilities and can only be approached using experiments with the shortcoming that only few velocity derivatives components are generally captured and that the probe spatial resolution might not be suited. One may thus need to explore the adequacy of the different surrogate

of ϵ in a range of Reynolds number for which experiments and simulation crossover. The most suited surrogate as inferred from DNS might then be used in experiments at a much higher value of Reynolds number.

The present work aims at assessing the performance of the ϵ-surrogates (Eqs. 2, 3, 5, 6, and 9) in the wake of a square cylinder (SqC) through direct numerical simulations. The emphasize is on the mean as well as instantaneous values of ϵ. The particular choice of the square cylinder is motivated by the fact that this geometry is easier to implement on numerical simulations. In addition, as shown by Thiesset et al.[34], a SqC generates a more isotropic wake that a CC, a screen, a plate and a screen strip. Accordingly, the SqC wake can be considered as an appropriate test case for above expressions of the ϵ-surrogates. One can, for example, expect a better agreement between $\overline{\epsilon}$ and $\overline{\epsilon}_{iso}$ for the SqC than for the other obstacles.

The lattice Boltzmann method for simulating the wake flow is first described in §II and calculations are validated in §III. In §IV and §V, a particular attention is paid on the mean and root mean square values of ϵ and compared to its surrogates for three downstream positions ($x = 20$, 60 and $100D$). Surrogates of $\overline{\epsilon}$ are studied in either the centerline and off centerline to appraise the effect of the mean shear. Then, the analysis is extended to the instantaneous values of ϵ in §VI, by means of comparative study of the probability density functions (PDF). To further assess the adequacy of using approximates for ϵ, joint probability density functions (JPDF) between ϵ and its surrogates are employed (§VII) yielding to a more stringent test. Finally, conclusion are drawn in §VIII.

II. LATTICE BOLTZMANN METHOD

The direct numerical simulation of the SqC wake is carried out using the lattice Boltzmann method (LBM). Rather than solving the governing fluid equations (Navier-Stokes equations), the LBM solves the Boltzmann equation for the probability distribution function $f_i(\overrightarrow{x}, t)$ on a lattice. The basic idea of the LBM is to construct a simplified kinetic model that incorporates the essential physics of microscopic average properties, which obey the desired (macroscopic) Navier-Stokes equations[15]. With a sufficient amount of symmetry of the lattice, the LBM implicitly resolves these latter equations with second-order accuracy. The

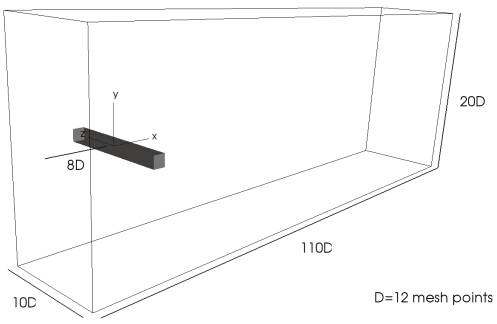

FIG. 1. Unscaled sketch of the computational domain

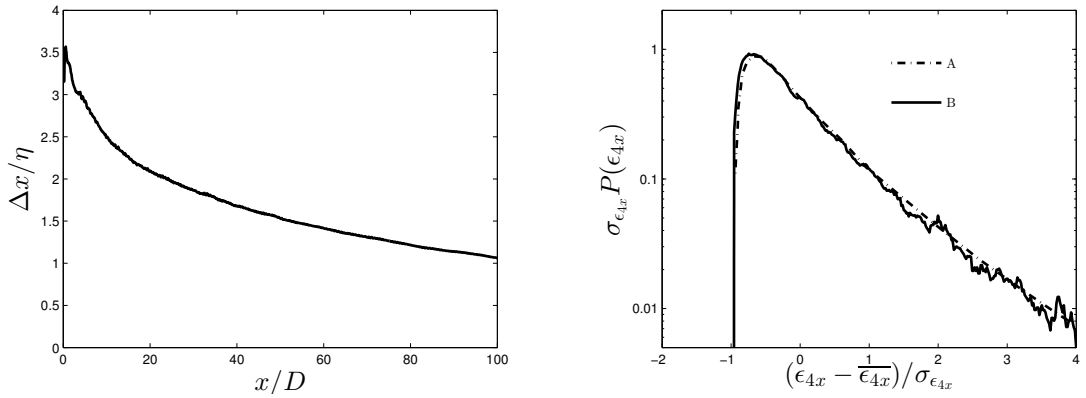

(a) (b)

FIG. 2. (a) Variation of $\Delta x/\eta$ with x along the axis of the SqC wake. (b) Probability density function of the turbulent kinetic energy dissipation inferred from Eq. (9) at $x/D = 100$ on the centerline. Solid line: present data (SC) ; dashed dotted line: DNS from Antonia et al.[3] using Eq. (9).

Boltzmann equation for $f_i(\overrightarrow{x}, t)$ is given by

$$\frac{f}{t} + \overrightarrow{e}\nabla_x f = \Omega \tag{10}$$

where $\overrightarrow{x}$ is the displacement vector, $\overrightarrow{e}$ is the particle velocity and Ω is a collision operator approximated by the Bhatnagar-Gross-Krook (LBGK) model

$$\Omega = \frac{1}{\tau}(f^{eq} - f), \tag{11}$$

where f^{eq} is an equilibrium particle distribution function and τ is the relaxation time. The

lattice Boltzmann equation, is then expressed as

$$f_i(\overrightarrow{x} + e_i\Delta t, t + \Delta t) - f_i(\overrightarrow{x}, t) = \Omega_i \\ = -\frac{1}{\tau}(f_i(\overrightarrow{x}, t) - f_i^{eq}(\overrightarrow{x}, t)) \tag{12}$$

Δt is the time step, $e_i(= \Delta x/\Delta t)$ is the velocity of the particle i in the i-direction; f_i^{eq} given by

$$f_i^{eq}(\overrightarrow{x}, t) = \rho\omega_i \left(1 + 3e_i\overrightarrow{u} + \frac{9}{2}(e_i\overrightarrow{u})^2 - \frac{3}{2}\overrightarrow{u}^2\right), \tag{13}$$

where ω_i is the corresponding weights for each i-direction and the macroscopic quantities ρ and u are the local fluid density and the local fluid velocity vector defined respectively by

$$\rho = \sum_i f_i \qquad ; \qquad \rho\overrightarrow{u} = \sum_i f_i e_i. \tag{14}$$

Using Eq. (14), Eq. (12) returns the Navier-Stokes equation with a second-order accuracy. In the collision term Ω_i (Eq. (11)), τ is related to the kinematic viscosity ν by

$$\nu = \frac{2\tau - 1}{6}. \tag{15}$$

The LBE is discretized on a Cartesian lattice, $\Delta x = \Delta y = \Delta z = 1$, and $\Delta t = 1$. A detailed description of the LBM can be found in Chen and Doolen (1998)[8] and Succi (2000)[30]. The motivation for the choice of the LBM over the resolution of the Navier-Stokes equations can be briefly summarised as follows: (i) extreme ease of solid surfaces implementation, (ii) no need for solving the Poisson equation for the pressure and (iii), which follows in parts from (ii), the collision is local in nature, making the implementation of parallel computation extremely easy. The method was successfully used for simulating turbulent flows[7,9–11,13].

III. VALIDATION OF COMPUTING

The three-dimensional computational Cartesian domain (Fig. 1) has $110D \times 20D \times 10D$ mesh points in the streamwise (x), across the wake (y), transversal (z) directions and $D = 12$ (D is the size of one side of the square section of the obstacle). The mesh increments in the three directions are equal, regular with $\Delta x = \Delta y = \Delta z = 1$. The center of the obstacle is located at $8D$ from the inlet and $10D$ from both top and bottom boundaries of the domain. The downstream distance extends to $x/D = 100$ when the origin of x is taken at the center of the cylinder.

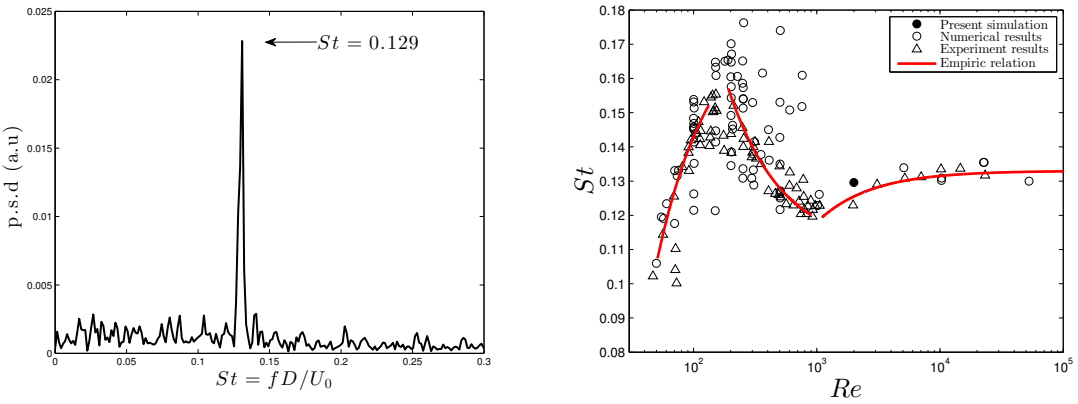

(a) (b)

FIG. 3. (a) Spectra of ϵ at $x/D = 20$ and $y/D = 4$. (b) Variation of the Strouhal number with the Reynolds number. Experimental results[12,23,26,28] ; Numerinal results[24,28]

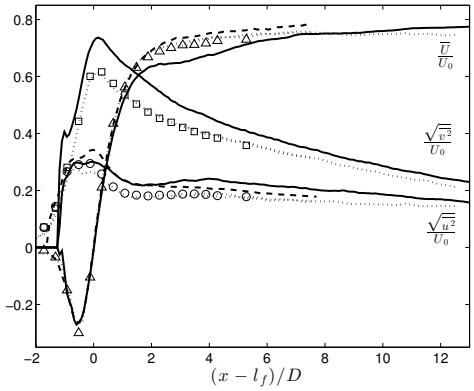

FIG. 4. Streamwise distributions of $\overline{U}/U_0$, u'/U_0 and v'/U_0, on the centerline of a CC wake. Solid line: LBM; dashed line: LES ; dotted line: PIV-2C[33]; symbols: ADL3C[33] measurements.

Periodic conditions are applied in the y and z directions. At the inlet, a uniform velocity ($U_{int} = 0.0833$ and $V_{int} = W_{int} = 0$) is imposed whilst a convective boundary condition is applied at the outlet of the domain. A no-slip condition at the wall is simulated with a bounce-back scheme, which means that, at the wall, the particles bounce back along the same direction. The Reynolds number $R_D = U_0 D/\nu$ is equal to 2000. This value is sufficiently small to allow a relatively good spatial resolution and sufficiently large to be comparable with previous experiments.

In order to avoid the occurrence of instabilities where the magnitude of the local strain

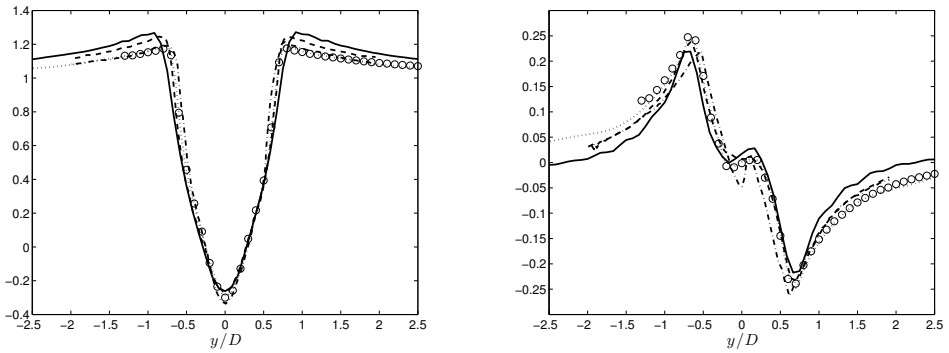

(a) $\overline{U}/U_0$ (b) $\overline{V}/U_0$

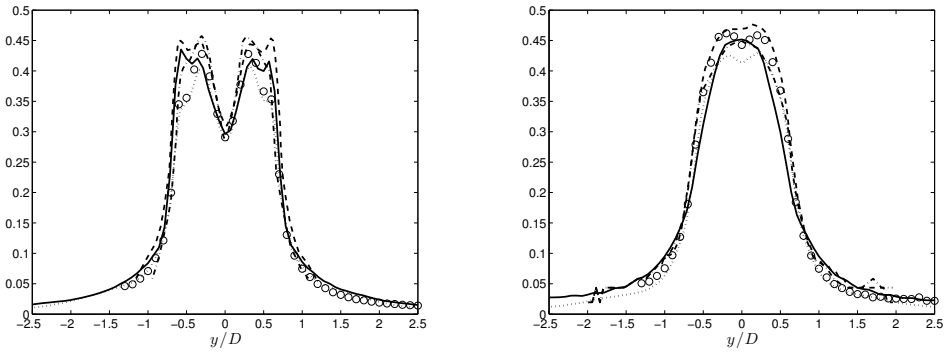

(c) u'/U_0 (d) v'/U_0

FIG. 5. Profiles of $\overline{U}$ (a), $\overline{V}$ (b), u' (c) and v' (d) at $x/D = 0.54$. Solid line: LBM; doted line: PIV-2C[33]; dashed-dotted line: DNS[27]; dashed line: LES[21]; symbols: ADL3C measurements[33].

rate could be large, mainly around the cylinder, a Large Eddy Simulation scheme (LES) based on the Smargorinsky model is used

$$\nu_{total} = \nu + \nu_\tau, \tag{16}$$

where ν_τ is the turbulent viscosity

$$\nu_\tau = (C\Delta)^2|S|, \tag{17}$$

where C is the Smagorinsky constant (=0.1), the cut-off separation $\Delta = \Delta x$ and $S = \sqrt{2S_{ij}S_{ij}}$ is the magnitude of the strain rate tensor (further details can be found in Djenidi, 2006[9] and Djenidi et al., 2013[11]).

An *a posteriori* check of the spatial resolution has been made and reveals that the computational mesh resolution which varies from about 3.5η at $x/D \simeq 1$ to 1η at $x/D \simeq 100$

(Fig. 2a) is comparable to many existing DNS[9,18,27]. Fig. 2b compares the present PDF of $(\epsilon_{4x} - \overline{\epsilon_{4x}})$ with that obtained in a 3D periodic turbulence box simulation[3] at $R_\lambda = 45$ using the same approximation for ϵ. The relatively good collapse of the two distributions provide confidence in the LBM simulations for capturing the small-scales. Note that this collapse supports the quasi-universality of the small-scale motion.

The flow visualisations (not presented here) showed the classical shedding of the Bénard - von Kármán vortices, with a Strouhal number $St = fD/U_0 = 0.129$ (f is the shedding frequency) as shown in Fig. 3a. This value of St is remarkably close to the experimental data of Okajima[26] who found $St = 0.13$ in a wake of SqC at $Re = 2000$.

To further assess the validity of the LBM simulation, we compare some of our results with existing experimental and numerical results obtained in the wake of a circular cylinder. There are fewer data for a SqC than a CC. Consequently, we carried out a LBM simulation of a CC to perform such comparison. Fig. 4 shows the normalized streamwise distributions of the mean velocity $\overline{U}$, the velocity fluctuations, u' and v' (the prime denotes the rms value) on the wake centerline; the normalisation is based on the length of the recirculation zone behind the cylinder, l_f, and the incoming velocity U_0. The LBM results are consistent with experimental[33] and LES[27] results at similar Reynolds numbers. For example, both the location and magnitude of the minimum value of $\overline{U}$ are well reproduced by the LBM. Also, the present LBM values of u' are in relatively good agreement with the measurement and LES data. However, there are some discrepancies between the LBM values of v' and the experiments. While the LBM predicts correctly the location of the maximum of v', the magnitude is overpredicted. This is yet to be explained, but the differences may be in part attributed to some differences in the initial conditions of both experiments and simulations. Fig. 5 shows the profiles of $\overline{U}$, $\overline{V}$, u' and v' at $x/D = 0.54$. The LBM data are in good agreement with published data[21,27,33] and capture well all features.

Altogether, the results indicate that the LBM simulation is adequate and reliable for investigating notably the dissipation rate behaviour in the wake of a cylinder.

IV. RESULTS FOR THE MEAN KINETIC ENERGY DISSIPATION RATE

The adequacy of the surrogates for estimating the kinetic energy dissipation rate is first investigated at the level of mean quantities. To this end, the distribution of $\overline{\epsilon}$ and its

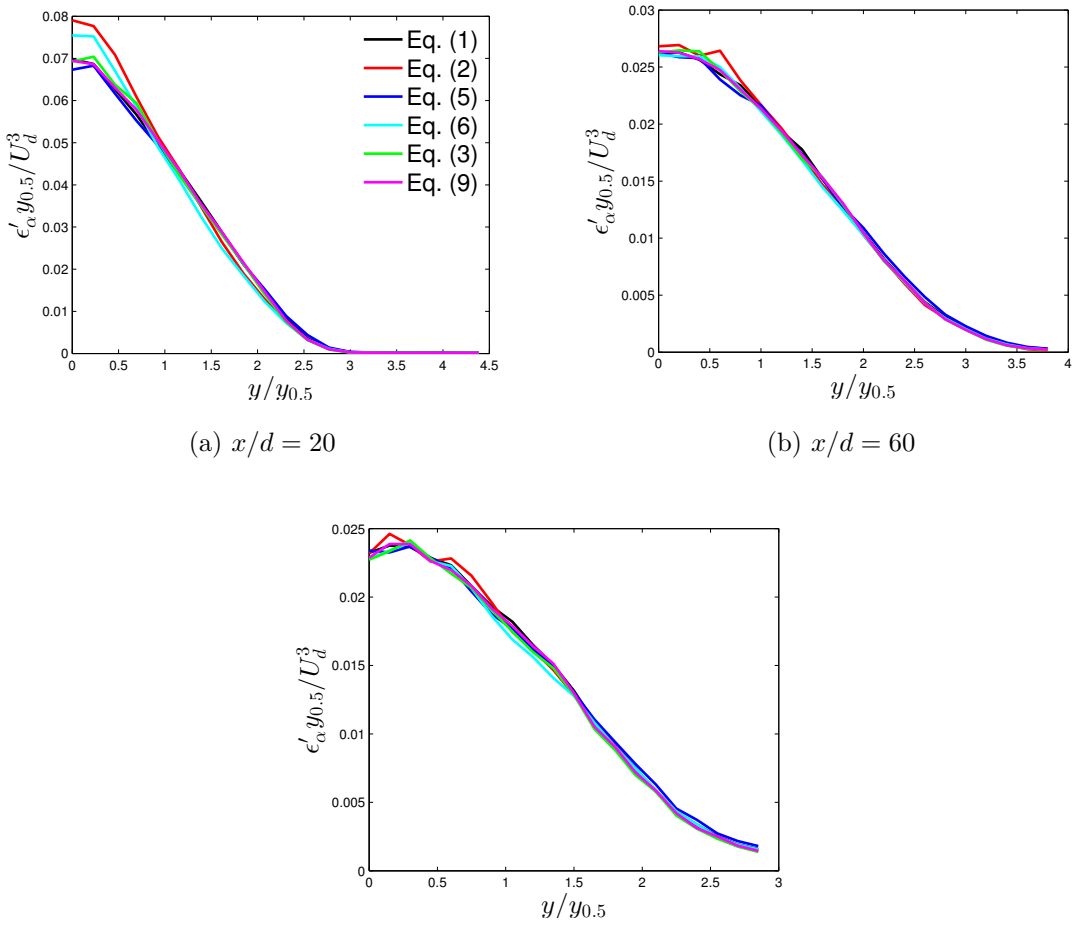

(a) $x/d = 20$

(b) $x/d = 60$

(c) $x/d = 100$

FIG. 6. Comparison of the mean dissipation rate of the turbulent kinetic energy dissipation across the wake.

surrogates at $x/D = 20$, 60 and 100 as a function of the transverse distance are displayed in figure 6. The normalization is based on the velocity defect U_d and the half-width $y_{0.5}$. Note first that by comparing these distribution at $x = 60D$ and $100D$, one observes that self-similarity is verified satisfactorily.

All distributions collapse well for $x/D = 60$ and 100 indicating that all the surrogates are adequate at these locations. However, this is no longer the case at $x/D = 20$ where the collapse excludes $\overline{\epsilon}_{iso}$ and $\overline{\epsilon}_{a,y}$. In particular, $\overline{\epsilon}_{iso}$ and $\overline{\epsilon}_{a,y}$ deviate significantly from the other distributions in the region $y/D \leq 1$. It is likely that the constraints imposed by these two expressions on the components of $\overline{\epsilon}$ are not satisfied in this region of the wake, not even on the wake centerline.

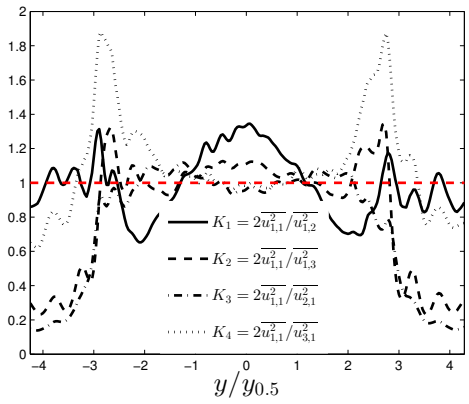

(a) K_1 to K_4

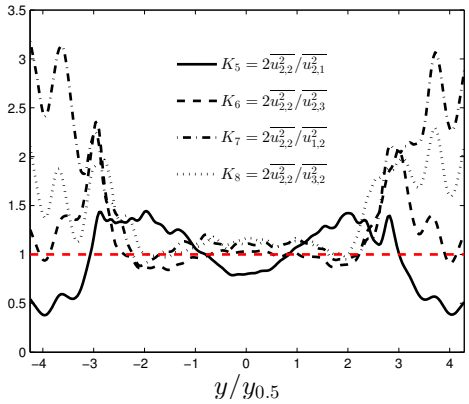

(b) K_5 to K_8

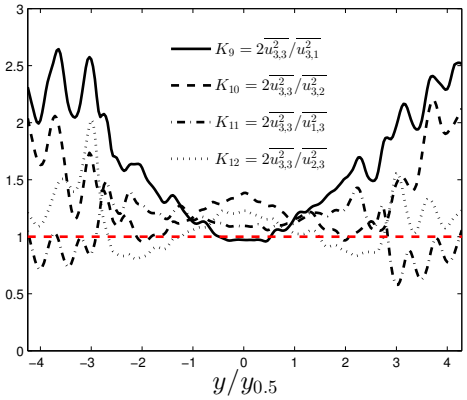

(c) K_9 to K_{12}

FIG. 7. Distributions across the wake of ratios K_1 to K_{12} at $x/D = 20$,(a) K_l to K_4, ; (b) K_5 to K_9 ; (c) K_9 to K_{12}. Red dashed , Isotropic value of 1.

The departure of $\overline{\epsilon}_{iso}$ from $\overline{\epsilon}$ at $20D$ is most probably caused by the anisotropy of the flow. To assess this issue, the velocity derivative ratios, $K = 2\overline{u_{i,j}}/\overline{u_{k,l}}$, are examined. Fig. 7, 8 and 9 show all the 12 ratios of the velocity derivatives involved in the expression of $\overline{\epsilon}$ for $x/D = 20$, 60 and 100, respectively; these ratios should be equal to one if isotropy is satisfied. On the wake centerline, the ratios K_1, K_2, K_5, K_{10} and K_{12} are larger than unity while the others are close to one for $x/D = 20$. At $x/D = 60$ and 100, except for K_1 all the ratios roughly agree with local isotropy on the centerline. Off the centerline, the ratios are closer to one for $x/D = 60$ and 100 than for $x/D = 20$. These results clearly indicate that anisotropy is stronger at $x/D = 20$ than at the other two locations and explain why $\overline{\epsilon}_{iso}$ differs markedly from $\overline{\epsilon}$ at $x/D = 20$.

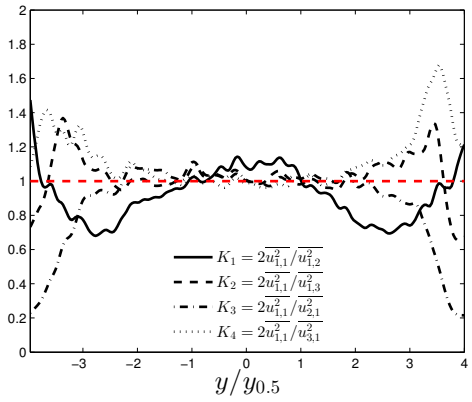

(a) K_1 to K_4

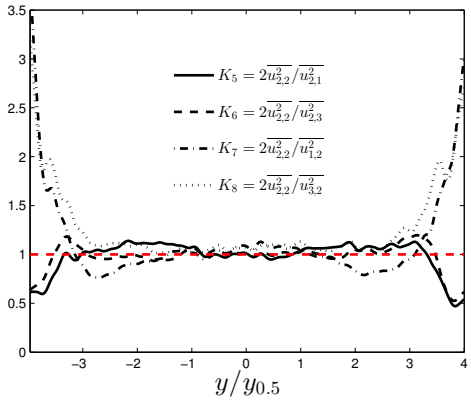

(b) K_5 to K_8

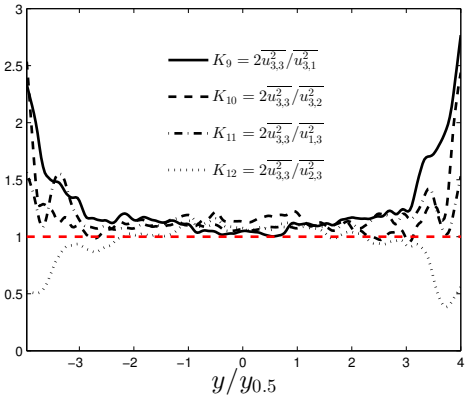

(c) K_9 to K_{12}

FIG. 8. Distributions across the wake of ratios K_1 to K_{12} at $x/D = 60$,(a) K_l to K_4, ; (b) K_5 to K_9 ; (c) K_9 to K_{12}. Red dashed line, Isotropic value of 1.

It is still remarkable that $\overline{\epsilon}_{iso}$ approximates $\overline{\epsilon}$ at $x/D = 60, 100$ considering that the flow is not isotropic, as illustrated by the departure of K_1 from one at all locations and across the wake width. Using three-component vorticity measurements, Antonia et al.[4] showed that there is a compensation effect in grid turbulence which explains the equality $\overline{\epsilon} = \overline{\epsilon}_{iso}$. These compensations appear to be at play also in the SqC wake flow in agreement with Ref. 34

In Ref. 4, they also noted satisfactory agreement between $\overline{\epsilon}$ and $\overline{\epsilon_{4x}}$, which they attributed to the fact that relation Eq. (8) was satisfied. A recent LBM simulation of grid turbulence (Djenidi and Antonia, 2013) confirms their argument. Unpublished DNS data in a turbulent channel flow[1,2] by Abe (Private communication) indicate that Eq. (8) is closely satisfied for $y/h \geq 0.1$ (y is the distance to the wall and h is the half-width of the channel). Figure 10

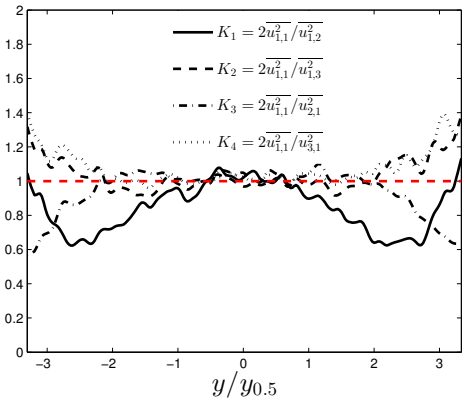

(a) K_1 to K_4

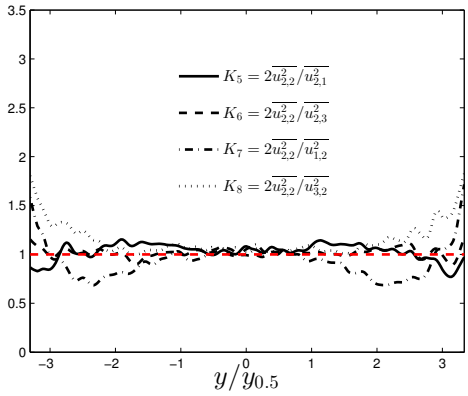

(b) K_5 to K_8

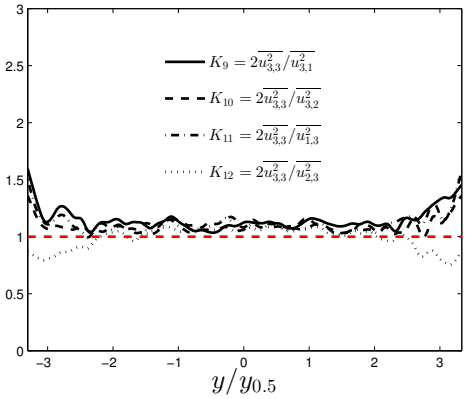

(c) K_9 to K_{12}

FIG. 9. Distributions across the wake of ratios K_1 to K_{12} at $x/D = 100$, (a) K_l to K_4; (b) K_5 to K_9; (c) K_9 to K_{12}. Red dashed line, Isotropic value of one.

shows that Eq. (8) is also valid in the present flow, in particular for $x/D = 60$ and 100. Clearly, the good collapse observed between $\overline{\epsilon}$ and its surrogates in the present flow shows that compensations are likely to be at play here, in particular away from the centerline where the departure from isotropy becomes important.

Although we cannot comment on the behaviour of $\overline{\epsilon}$ and its surrogates in the far wake, it is worth briefly recalling previously published results. As stated in the introduction, Browne et al.[6] found that the measured $\overline{\epsilon}_{iso}$ departed significantly (about 45% on the wake centerline and about 80% near the wake edge) from $\overline{\epsilon}$ obtained by measuring nine of its terms and assuming isotropy to infer the remaining three terms. They argued that this latter assumption is unlikely to be critical as they expected the magnitude of those terms

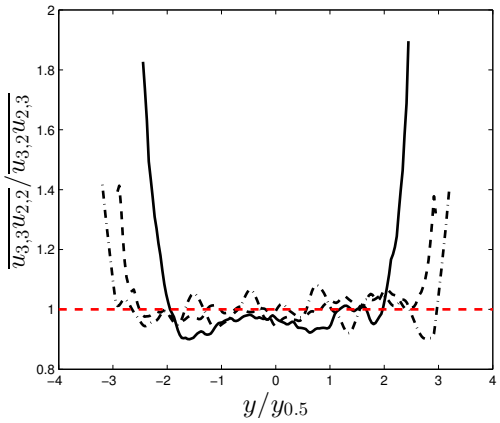

FIG. 10. Distributions across the wake of $\overline{u_{2,2}u_{3,3}}/\overline{u_{2,3}u_{3,2}}$ involved in Eq. (8) at $x = 20D$ (solid line), $60D$ (dashed line) and $100D$ (dot-dashed line). Red dashed line: Isotropic value of 1.

to be small by comparison with the other nine. The reasonable closure of their turbulent kinetic energy budget suggests that they measured $\bar{\epsilon}$ with adequate accuracy. However, Hao et al.[35] measured $\bar{\epsilon}_{ap} = \nu(6\overline{u_{,x}^2} + 3\overline{u_{,y}^2} + 2\overline{v_{,x}^2} + 2\overline{u_{,y}v_{,x}})$ (they assumed local isotropy and homogeneity, and the continuity equation) and observed that $\bar{\epsilon}_{iso}$ was only about 6% smaller than $\bar{\epsilon}_{ap}$ across the wake at $x/D = 420$). Unfortunately, these authors did not verify whether or not the measured $\bar{\epsilon}_{ap}$ closed the turbulent kinetic energy budget. Clearly, the discrepancy between the Browne et al.[6] and the Hao et al.[35] results requires further investigation, preferably via DNS. It should be noted however that whereas Browne et al. estimated the mean squared values of $u_{i,j}$ from 2-points correlations as $r \to 0$, Hao et al.[35] applied spectral corrections based on local isotropy, which may have introduced a systematic bias in their results and led to the close agreement between $\bar{\epsilon}_{iso}$ and $\bar{\epsilon}$.

V. STANDARD DEVIATION OF THE ENERGY DISSIPATION RATE

As far as fluctuating quantities are concerned, one can for example investigate the distribution of the standard deviation of ϵ across the wake. These are reported in Fig. 11 for $x = 20, 60$ and $100D$. Here again, use was made of appropriate combinations of the velocity defect U_d and the half-width $y_{0.5}$ to normalize these quantities.

Noticeable is the fact that, independently of x and the surrogate under consideration, the standard deviation of ϵ is of same magnitude as its mean value. This indicates that

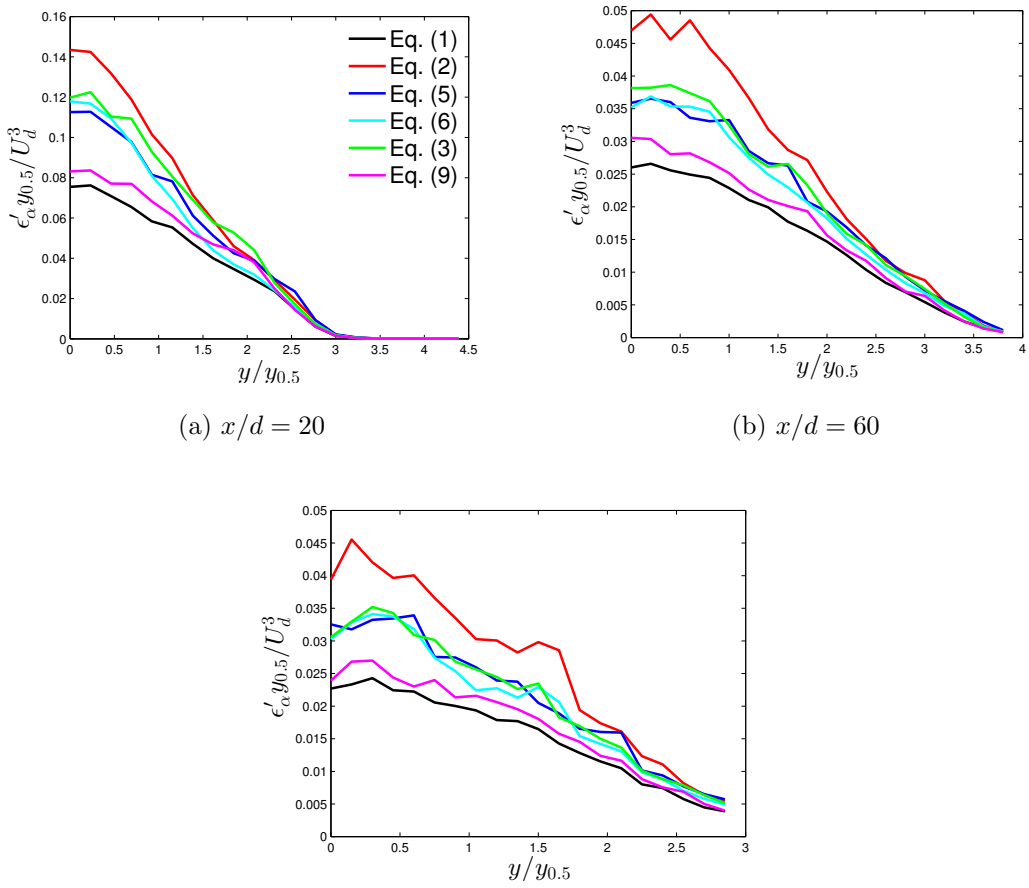

(a) $x/d = 20$

(b) $x/d = 60$

(c) $x/d = 100$

FIG. 11. Comparison of the root mean square dissipation rate of the turbulent kinetic energy dissipation across the wake.

the dissipation rate is a highly fluctuating quantity, in the same way - if not more - as any other fluctuating quantity, in agreement with Landau's comment. This remarks is of major importance in the context of refining the theoretical description of turbulence that may therefore account for the fluctuating nature of the dissipation rate.

Another remark concerns self-similarity of ϵ' when normalized by an appropriate set of variables. Indeed, it appears that self-similarity of ϵ is attained at the level of the standard deviation at $x = 60D$, *i.e.* at the same distance as for the mean value.

A careful analysis of Fig. 11 further reveals that, irrespectively of the downstream position, ϵ' is relatively well approximated by ϵ'_{4x}. Then, the best candidates appear to be the two axisymmetric expressions Eqs. (5) and (6) followed by the homogeneous surrogate Eq. (3) which altogether reveal a maximum departure from the real values of about 40-50%.

Finally, the use of the isotropic expression Eq. (2) systematically overestimates the standard deviation of ϵ by almost a factor 2.

In summary, whilst the ϵ_{4x} appears to be the best candidate for capturing the fluctuations of ϵ, the use of the isotropic surrogate leads to some drastic errors. This is particularly important when internal intermittency corrections which account for the fluctuating nature of the dissipation rate have to be applied. This is a remarkably challenging task since ϵ_{4x} requires measurements using a probe consisting of at least 4 X-wires.

It is worth mentioning that the fact that the standard deviation of ϵ_{4x} is in close agreement with that of ϵ does not necessarily imply that their respective probability density functions shape similarly. In the next section, we turn our attention to this issue.

VI. PROBABILITY DENSITY FUNCTION

The results of the preceding section showed that the kinetic energy dissipation rate can be relatively closely approximated by some of its surrogates at the level of mean quantities. However some departures from the real values of the dissipation rate were observed as regards to the standard deviation of this quantity. This is of significant importance from an experimental point of view, as one can be confident in estimating $\bar{\epsilon}$ from a limited set of measurements of velocity derivatives, whilst ϵ' requires more complex measurements.

However, the results do not give any indigent information on how the instantaneous values of the surrogates compare with ϵ. Some of this information can be obtained through the probability density function (PDF), shown in figure 12. The normalization of the PDF is such that $\int_{-\infty}^{\infty} P_\alpha d\alpha = 1$, where P_α is the PDF of α, and α represents ϵ and its surrogates. The figure also reports the PDF of ϵ obtained from the DNS data of decaying three-dimensional box turbulence[3].

All the PDFs present a similar positive tail with a nearly exponential form,

$$P_\alpha \sim exp(-\beta\alpha), \tag{18}$$

where the constant β is estimated to be about 1.25. However, significant differences in the PDFs are visible for $\alpha \leq 0$ at all x/D positions. For example, all the surrogate distributions depart from the PDF of ϵ at $x/D = 20$ and 60. Similar results were observed in grid turbulence[4] and a turbulent plane wake[36] (Zhu and Antonia, 1997). This means that the

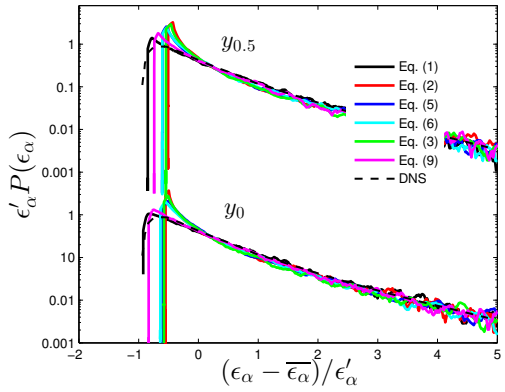

(a) $x/d = 20$

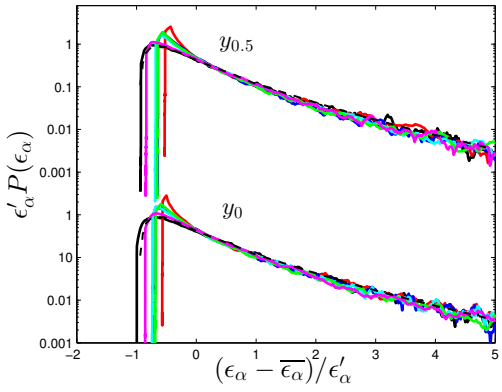

(b) $x/d = 60$

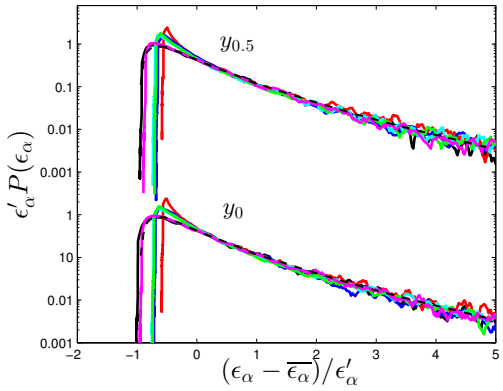

(c) $x/d = 100$

FIG. 12. Comparison of the probability density function of the turbulent kinetic energy dissipation at two different transverse positions $y = 0$ and $y = 0.5(P(\epsilon_\alpha) * 100)$. Black: ϵ; red: ϵ_{iso}; blue: $\epsilon_{a,x}$; light blue: $\epsilon_{a,y}$; green: ϵ_{hom} ; purple: ϵ_{4x}; The dashed line is the PDF of ϵ from the DNS[3] of a decaying box turbulence and is shown for reference.

error that one makes using surrogates of ϵ will be observed for the most probable values of ϵ and are therefore of critical importance.

Of all the surrogate PDFs for P_ϵ, only $P_{\epsilon_{4x}}$ closely follows P_ϵ; the agreement between the two is satisfactory at $x/D = 100$. This indicates that ϵ_{4x} captures well all instantaneous events ranging from weak to high intensity, and explains the good agreement observed earlier results not only, associated with their mean values (figure 6) but also their *rms* distributions (figure 11). This remark holds irespectively of the transverse distance y suggesting that there is no particular effect of the mean shear on the PDFs.

VII. JOINT PDFS

A more stringent test of the adequacy of the surrogates to estimate instantaneous values of ϵ can be further assessed using Joint PDF. Indeed, a joint PDF highlights the probability to observe a particular value of ϵ inferred from one particular surrogate knowing the real value of ϵ. They are thus likely to be more severe in assessing the adequacy of such surrogates.

The agreement between P_ϵ and $P_{\epsilon_{4x}}$ is well reflected in the JPDFs of ϵ and ϵ_{4x} shown in Figure 13, which also shows the JPDFs between ϵ and the other surrogates. These JPDFs are obtained on the centerline of the cylinder wake at $x/D = 100$. A perfect correlation between two variables α_1 and α_2 would be represented by a straight line $\alpha_1 = \alpha_2$ inclined at 45^0. Note that although none of JPDFs display a perfect correlation, the JPDF isocontours of ϵ and ϵ_{4x} reveal the best alignment along a 45^0 direction highlighting the reasonable agreement between P_ϵ and $P_{\epsilon_{4x}}$.

Moreover, there is some degree of correlation between ϵ and its other surrogates. This can be further assessed from the data of table I, which reports the correlation coefficients between ϵ and its surrogates ($\rho_{\epsilon,\alpha}$, α represents any of the surrogates) at $x/D = 100$ on the centerline and at half-width location. As expected, $\rho_{\epsilon,\epsilon_{4x}}$ is the largest. Antonia et al.[4] measured a coefficient $\rho_{\epsilon,\epsilon_{hom}}$ of about 0.8 in grid turbulence. They argued that a larger value would have been expected, had they been able to correct the instantaneous fluctuations for spatial resolution. However, with a value of about 0.61, the present $\rho_{\epsilon,\epsilon_{hom}}$ is not as large as that in grid turbulence. This indicates that the correlation between the energy dissipation rate and the enstrophy fields is weaker in the wake flow than in grid turbulence. In other words, this highlights a stronger effect of pressure fluctuations in the inhomogeneous wake flow by comparison to homogeneous grid turbulence.

Nevertheless, the fact that all the coefficients exceed 0.60 may indicate a non-negligible level of correlation between ϵ and its surrogates in general, regardless of the lateral position in the wake.

VIII. CONCLUSIONS

The instantaneous turbulent kinetic energy dissipation rate, ϵ, and its mean distributions, $\bar{\epsilon}$, in a wake of a square cylinder were investigated using numerical simulations based on

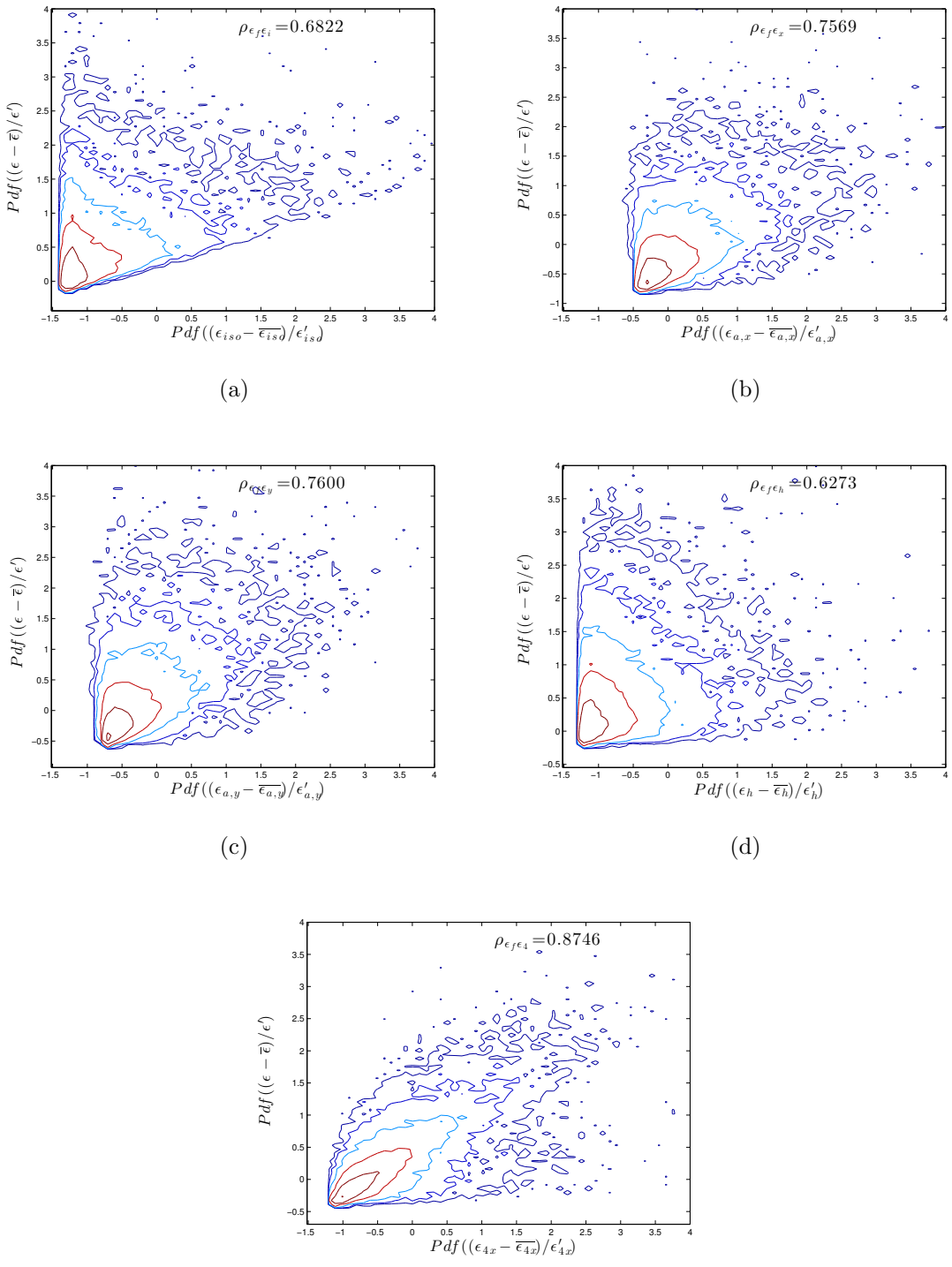

FIG. 13. Joint probability density function of the turbulent kinetic energy dissipation (Eq. (1) and Eq. (2), (5), (6), (3), (9) at position $y = 0$ and $x/D = 100$.

the lattice Boltzmann method. Various expressions for approximating $\overline{\epsilon}$, based on local

	$y=0$	$y_{0.5}$
$\rho_{\epsilon\epsilon_{iso}}$	0.68	0.68
$\rho_{\epsilon\epsilon_{a,x}}$	0.75	0.674
$\rho_{\epsilon\epsilon_{a,y}}$	0.76	0.78
$\rho_{\epsilon\epsilon_{hom}}$	0.62	0.61
$\rho_{\epsilon\epsilon_{4x}}$	0.87	0.85

TABLE I. Correlation coefficient $\rho_{\epsilon\epsilon_{iso}}$, $\rho_{\epsilon\epsilon_{a,x}}$, $\rho_{\epsilon\epsilon_{a,y}}$, $\rho_{\epsilon\epsilon_{hom}}$ and $\rho_{\epsilon\epsilon_{4x}}$ at $x/D = 100$

isotropy (ϵ_{iso}), local axisymmetry along x ($\epsilon_{a,x}$) and y ($\epsilon_{a,y}$), local homogeneity (ϵ_{hom}), and homogeneity in the transverse plane, (ϵ_{4x}), were assessed as surrogates for ϵ.

All the approximations show a good collapse with $\overline{\epsilon}$ when the distance downstream of the cylinder is larger than about 40 diameters. Even thought $\overline{\epsilon}_{iso}$ is suited for such distance, it was shown that compensation between the components of ϵ are at play and explains the latter agreement between $\overline{\epsilon}_{iso}$ and $\overline{\epsilon}$ Closer to the cylinder, the collapse is reasonable across the wake, except for $\overline{\epsilon}_{iso}$ and $\overline{\epsilon}_{a,y}$, which depart from $\overline{\epsilon}$ in the region $0 \leq y/D \leq 1$.

The analysis is then extended to the instantaneous values of ϵ using PDFs and JPDFs. It is emphasized that ϵ_{4x} correlates best with ϵ whereas ϵ_{iso} shows the smallest correlation with ϵ.

In summary, results indicate that ϵ_{4x} (Eq. (9) is an adequate surrogate for ϵ and can be used for correctly determining the probabilistic behaviors of ϵ. This have a major importance for experimentalists since a reliable estimate of the instantaneous properties of the kinetic energy dissipation rate.

REFERENCES

[1]Abe, H., Antonia, R., and Kawamura, H., "Correlation between small-scale velocity and scalar fluctuations in a turbulent channel flow," J. Fluid Mech **627**, 1 – 32 (2009).

[2]Antonia, R., Abe, H., and Kawamura, H., "Analogy between velocity and scalar fields in a turbulent channel flow," J. Fluid Mech. **628**, 241 – 268 (2009).

[3]Antonia, R., Orlandi, P., and Zhou, T., "Assessment of a three-component vorticity probe in decaying turbulence," Expts Fluids **33**, 384 – 390 (2002).

[4]Antonia, R. A., Zhou, T., and Zhu, Y., "Three-component vorticity measurements in a turbulent grid flow," J. Fluid Mech. **374**, 29 – 57 (1998).

[5]Aronson, D. and Lofdahl, L., "The plane wake of a cylinder: Measurements and inferences on turbulence modeling," Phys. Fluids **5**, 1433 (1993).

[6]Browne, L. W. B., Antonia, R. A., and Shah, D. A., "Turbulent energy dissipation in a wake," J . Fluid Mech. **1 79**, 307 – 326 (1987).

[7]Burattini, P., Lavoie, P., Agrawal, A., Djenidi, L., and Antonia, R. A., "Power law of decaying homogeneous isotropic turbulence at low reynolds number," Phys Rev E **73** (2006).

[8]Chen, S. and Doolen, G. D., "Lattice boltzmann method for fluid flows," Ann. Rev. Fluid Mech. **30**, 329 – 364 (1998).

[9]Djenidi, L., "Lattice-boltzmann simulation of grid-generated turbulence," J. Fluid Mech. **552**, 13 – 35 (2006).

[10]Djenidi, L., "Structure of a turbulent crossbar near-wake studied by means of lattice boltzmann simulation," Phys Rev E **77** (2008).

[11]Djenidi, L., Tardu, S. F., and Antonia, R. A., "Relationship between temporal and spatial averages in grid turbulence," J. Fluid Mech. **730**, 593 – 606 (2013).

[12]Durao, D. F. G., Heitor, M. V., and Pereira, J. C. F., "Measurements of turbulent and periodic flows around a square cross-section cylinder," Expts Fluids **6**, 298 – 304 (1988).

[13]Ertunc, O., Zyilmaz, N. O., Lienhart, H., Durst, F., and Beronov, K., "Homogeneity of turbulence generated by static-grid structures," J. Fluid Mech. **654**, 473 – 500 (2010).

[14]Fabris, G., *Conditionally sampled turbulent thermal and velocity fields in the wake of a warm cylinder and its interaction with an equal cool wake*, Ph.D. thesis, Illinois Institute of Technology (1974).

[15]Frisch, U., Hasslacher, B., and Pomeau, Y., "Lattice-gas automata for the navier-stokes equation," Phys Rev E Letters **56,14** (1986).

[16]George, W. and Hussein, H., "Locally axisymmetric turbulence," J Fluid Mech **233**, 1 – 23 (1991).

[17]Hussein, H. J., "Evidence of local axisymmetry in the small scales of a turbulent planar jet," Phys. Fluids **6**, 20 – 58 (1994).

[18]Kaneda, Y., Ishihara, T., Yokokawa, M., Itakura, K., and Uno, A., "Energy dissipation rate and energy spectrum in high resolution direct numerical simulations of turbulence in

a periodic box," Phys. Fluids **15** (2003).

[19]Kolmogorov, A. N., "Dissipation of energy in the locally isotropic turbulence," Doklady Akademii Nauk SSSR **32**, 16 (1941).

[20]Kolmogorov, A. N., "The local structure of turbulence in incompressible viscous fluid for very large reynolds number," Doklady Akademii Nauk SSSR **30**, 301 (1941).

[21]Kravchenkoa, A. G. and Moin, P., "Numerical studies of flow over a circular cylinder at re=3900," Phys. Fluids **12** (2000).

[22]Landau, L. D. and Lifshitz, E. M., *Fluid Mechanics* (Pergamon Press, London., 1959).

[23]Lee, B. E., "The effect of turbulence on the surface pressure field of a square prism," J. Fluid Mech. **69**, 263 – 282 (1975).

[24]Liu, T., Liu, G., Ge, Y., Wu, H., and Wu, W., "Extended lattice boltzmann equation for simlation of flows around bluff bodies inhight reynolds number," in *BBAA VI International Colloquium on: Bluff Bodies Aerodynamics & Applications Milano, Italy, July, 20-24* (2008).

[25]Mi, J. and Antonia, R. A., "Approach to local axisymmetry in a turbulent cylinder wake," Expts Fluids **48**, 933 – 947 (2010).

[26]Okajima, A., "Strouhal numbers of rectangular cylinders," J Fluid Mech **123**, 379 – 398 (1982).

[27]Parnaudeau, P., Carlier, J., Heitz, D., and Lamballais, E., "Experimental and numerical studies of the flow over a circular cylinder at reynolds number 3900," Phys. Fluids **20** (2008).

[28]Sohankar, A., Norberg, C., and Davidson, L., "Simulation of three-dimensional flow around a square cylinder at moderate reynolds numbers," Phys. Fluids **11**, 288 (1999).

[29]Sreenivasan, K. R. and Antonia, R. A., "The phenomenology of small-scale turbulence," Ann. Rev. Fluid Mech **29**, 435 – 472 (1997).

[30]Succi, S., *The lattice Boltzmann equation: for fluid dynamics and beyond*, edited by O. university press (2001).

[31]T. Zhou, Z. Hao, L. P. C. and Zhou, Y., "Comparisons between different approximations to energy dissipation rate in a self-preserving far wake," Phys Rev E **74** (2006).

[32]Taylor, G. I., "Statistical theory of turbulence," Proc. R. Soc. Lond. A **151**, 422 (1935).

[33]Thiesset, F., *Exploration analytique et exprimentale des interactions cohrence-turbulence au sein dun coulement de sillage*, Ph.D. thesis, Faculte des Sciences & Techniques de

lUniversite de Rouen (2011).

[34]Thiesset, F., Danaila, L., and Antonia, R. A., "Dynamical effect of the total strain induced by the coherent motion on local isotropy in a wake," J. Fluid Mech. **720**, 393 – 423 (2013).

[35]Z. Hao, T. Z., Chua, L., and Yu, S., "Approximations to energy and temperature dissipation rates in the far field of a cylinder wake," Experimental Thermal and Fluid Science **32**, 791 – 799 (2008).

[36]Zhu, Y. and Antonia, R., "On the correlation between enstrophy and energy dissipation rate in a turbulent wake," Applied Scientific Research **57**, 337 – 347 (1997).